ISSN 0915-633X

NATIONAL INSTITUTE FOR FUSION SCIENCE

Design Study of the Large Helical Device

A. Iiyoshi, M. Fujiwara, O. Motojima, J. Todoroki, N. Ohyabu
and K. Yamazaki

(Received — Nov. 1, 1989)

NIFS-1 Jan. 1990

RESEARCH REPORT
NIFS Series

NAGOYA, JAPAN

Design Study of the Large Helical Device

A. Iiyoshi, M. Fujiwara, O. Motojima,
J. Todoroki, N. Ohyabu and K. Yamazaki

National Institute for Fusion Science
Nagoya, 464-01 Japan

Abstract

The Large Helical Device (LHD) is a Heliotron/torsatron type superconducting helical fusion device, which is scheduled to be constructed by the newly established National Institute for Fusion Science as the major joint-university fusion research project.
This report describes the design study of the LHD. Our goal is demonstration of high energy confinement and high β in the helical device, which is a necessary step toward a helical reactor system.

Keywords : helical device, currentless steady state experiment, Superconducting device.

1. INTRODUCTION

Significant progress has recently been made in research on helical devices (stellarators, heliotrons, torsatrons)[1]. Both experimental and theoretical studies have shown that this is a very promising fusion reactor concept. But its development lags behind that of the tokamak. This is because the rotational transform in the tokamak configuration is generated efficiently by current flowing through the plasma, therefore it is less expensive to build a larger tokamak device. However, the next major physics issues for the tokamak research are related to the plasma current, efficient non-ohmic current drive and prevention of major plasma current disruptions. These issues must be resolved before a tokamak reactor can be designed.

In helical devices, on the other hand the confining magnetic fields are generated by the external coils and thus helical devices are free of the above mentioned tokamak problems. This inherent advantage makes the helical concept very attractive. It has been demonstrated by small scale helical device experiments that the plasma performance in helical devices is comparable to that of a comparable tokamak device. In order to examine whether a helical device is a viable candidate for a fusion reactor system, a large-scale helical device comparable to the present day tokamak device is needed. We propose to construct a superconducting large helical device (Heliotron/torsatron type, ℓ=2, m=10, γ_c=1.2, B=4T, R=4m). An overview of the proposed device is shown in Fig.1 (a) and (b). Both the helical coils and poloidal coils are designed to be superconducting coils. Experimental facilities for the device, illustrated in Fig.1(c) will be located at Toki, a small town near Nagoya.

The budget for the first year of the seven year construction period has been approved by the Japanese government April 1989 and its construction schedule is shown in table 1.

We report here a summary of our design study of the LHD. Since our design study is still on-going, new thinkings or ideas will be added as the design is refined. In Section 2, the objectives of the project are discussed. In Section 3 , we describe goals of the plasma performance and design criteria for the magnetic

configuration. Section 4 discusses the helical divertor, a major feature of the proposed device. Heating systems in the proposed device are presented in Section 5. Experimental plan of the proposed device is described in Section 6.

2. OBJECTIVES OF THE PROJECT

Ther overall objective of this project is to clarify the physics and engineering issues important in designing a future helical reactor by studying the behavior of currentless plasmas in the large-scale experimental helical device. This research project will be carried out as the major Japanese university fusion research project.

The major goals to be pursued:

(a) To carry out a wide range of studies on the transport under high n τ T plasma conditions that can be extrapolated to reactor plasmas.

(b) To achieve high-beta plasmas with a average beta value of >5%, as needed for a reactor, and to understand the related physics.

(c) To obtain the basic data necessary to realize steady-state operation through experiments on the quasi-steady plasma control using a divertor.

(d) To study the behavior of high-energy particles in the helical magnetic field and to conduct α particle simulation experiments.

(e) To increase the comprehensive understanding of toroidal plasmas by carring out studies complementary to those in tokamaks.

3. TARGET PLASMA AND DESIGN CRITERIA FOR MAGNETIC CONFIGURATION

The following target plasma values and device parameters are adopted for conducting the above-mentioned research.

Plasma Parameters:

CASE 1 : (high n τ T) T_i = 2 - 4keV, $\bar{n}_e = 10^{20}$ m^{-3},
τ_E = 0.1 - 0.3 sec, B = 4T,

CASE 2: Ti(0) = 10keV, $\bar{n}_e = 2 \times 10^{19}$ m^{-3},
(high T_i) τ_E = ~ 0.1 sec, B = 4T,
CASE 3: $\bar{\beta}$ (average beta value) $\gtrsim$ 5%, B = 0.5 ~ 1T.
(high β)

Device Parameters:

a_p(minor radius of the plasma) = (50-60)cm, R/a_p= 8-9
R = ~ 4m
B = 4T, P_{abs} = 15-20MW

The magnetic field configuration is optimized through various physics considerations.

The ℓ = 2 heliotron/torsatron configuration is adopted as the magnetic configuration because of its well established data base. This configuration has a built-in divertor, which is one of the important features of this program.

Configurations for obtaining high beta are studied with MHD codes (H-APOLLO, H-ERATO) using the stellarator approximation method under the net currentless plasma equilibrium condition. Various parameters reflecting the geometrical shape of coils, $A_c=R/a_c$, m, γ_c = (m/ℓ) (a_c/R), are varied widely to find the optimum magnetic configuration, where R, a_c and m are the major radius, minor radius and the pitch number of the helical coil, respectively.

Figure 2 shows the parameter space where $\bar{\beta} \gtrsim 5\%$ is attainable. (a) In the case of m = 10, $\bar{\beta}\sim$ 5% is attainable if $\gamma_c > 1.2$. (b) In the case of m=14, $\bar{\beta}\gtrsim$ 5% is attainable if $\gamma_c > 1.29$. (c) In the case of FCT equilibrium, the critical beta value is lower.

An inward shift of the plasma improves the equilibrium beta limit because of an increase in ι and a decrease in the axis shift (in vacuum), and the stability beta limit also increases until a sudden loss of stability for interchange modes due to the loss of the magnetic well (Fig.3)[2]. For m=10 / γ_c = 1.20 / R=4m configuration, the stability beta limit of 5% is achieved when the plasma is shifted about 15cm inwards (Fig.3a); If the plasma inward shift is less than this value, the beta limit is restricted by the equilibrium. For m=14 /γ_c = 1.29 configuration, beta-limit ~ 3% is

obtained; this value is less than the equilibrium limit (Fig.3(b)). When the plasma is moved outwards, the beta limit is restricted by a ballooning mode type instability. We have also studied the improvement of the plasma stability caused by quadrupole, and hexapole magnetic fields.

With smaller γ_c values, the helical ripple ε_h and S_p/S_c ($S_p = \pi a_p^2$, $S_c = \pi a_c^2$) can be smaller, as shown in Fig.4. A smaller ε_h lowers the diffusion caused by the helical ripple. A smaller s_p/s_c results in a larger distance between the helical coil and the plasma boundary (the separatrix surface).

Confinement scalings for evaluating the target plasma values (Fig.5) and device parameters are as follows:

a) Empirical scalings obtained from the results of experiments on helical devices [3],

$$\tau_E^{EMP1} = 0.17 P_{abs}^{-0.58} \bar{n}_e^{0.69} B^{0.84} a^{2.0} R^{0.75}$$

(S) (MW) ($10^{20}m^{-3}$) (T) (m) (m)

$$\tau_E^{EMP2} = 0.21 P_{abs}^{-0.53} \bar{n}_e^{0.66} B^{0.53} a^{2} R$$

b) Confinement scaling based on neoclassical theory and the additional anomalous transport (based on the analysis of ECH and NBI plasmas in Heliotron E) [4].

Scaling (b) predicts the following plasma energy confinement. (1) In the low-density region ($n_e \lesssim 3 \times 10^{19}m^{-3}$), it is easy to realize the condition for the electron root (plasma radial electric field $E_r > 0$). As a result, $T_i(0) > 10keV$ will be achieved with $P_{abs} \gtrsim 15MW$ and $a_p \gtrsim 50cm$.

(2) The high-density region ($\bar{n}_e \sim 10^{20}m^{-3}$) produces the ion root ($E_r<0$), and $T_i(0) = 4 - 5keV$ is obtained when $P_{abs} \gtrsim 15MW$ and $a_p \gtrsim 50cm$. Plasmas with a high $n\tau T$ value are obtained as a result of an expected $\tau_E = 0.1 - 0.3$ sec.

Orbit loss of fast ions is a concern for a helical magnetic configuration. Drift orbit calculations have been carried out by using both real coordintes and magnetic coordinates, both for vacuum magnetic field and for more realistic field in finite beta plasmas incorporated with MHD calculations. The drift surface of passsing particles can be controlled by the magnetic surface, while the position of the drift surfaces for locally-trapped paarticles are controlled by the mod-B structure. The good confinement is

realized by adjusting these two structures. The magnetic surface can be moved by the vertical field, and the mod-B structure can be modified by pitch modulation. The particle loss diagram for different position of the magnetic axis are shown in Fig.6(a) for the m=10 configuration. The particles are assumed to be lost when they reach the outermost magnetic surface. The particle loss fraction, defined as the ratio of the lost particle number to the total number within the outermost magnetic surface in pitch angle and major radius space, versus the shift of the magnetic axis are shown in Fig.6(b) for m=10 and m=14. The particle loss fraction can be reduced effectively by an inward shift of the magnetic axis,

In order to study long-pulse, currentless plasmas, various divertor actions are necessary for controlling impurities, particle flux, and heat flux. It may also improve the energy confinement (H-mode). For m=10, slight pitch modulation of the helical coils is desirable for providing a clear separatrix configuration outside the outermost closed magnetic surface. On the other hand, the standard configuration is adequate for creating the separatrix when m=14.

Based on the above-mentioned results we have selected the following coil systems for design work.

γ_c = 1.20 - 1.30, m=10, 12 and 14

During the preliminary design of the main device, the m=10 case is extensively studied [5, 6]. The coil configuration will be finalized in the detailed design phase by taking into account experimental results from Heliotron E, ATF and CHS.

4. DIVERTOR DESIGN STUDY

The helical Divertor is one of the major features of the proposed LHD. We discuss the design rationale for the divertor and its conceptual design. The main objective of the LHD is to achieve high quality plasma for a long period. This necessitates (1) minimization of impurity contamination, (2) reduction of the heat load on the divertor plate, (3) improvement of the energy confinement time. We believe that the above fuctions could be met by installing a proper divertor in the device.

The magnetic field configuration of the helical divertor is rather complex and thus needs to be studied carefully before designing the divertor system. Fig.7 shows divertor magnetic configurations for the LHD (ℓ=2, m=10, γ_c=1.2, R=4m). As shown in this figure there exists an ergodic region just outside the outermost closed surface, which is created by overlapping of the island layers with a toroidal mode number of 10.

Field lines escaping from the ergodic region deviates radially from the ergodic region before reaching to the divertor plate. This radial deviation is larger for less helically symmetric configuration (smaller coil pitch modulation (α) and smaller inward shift of the plasma axis ($-\Delta$)). This radial deviation aggravates the design problem of clearance between the edge plasma and the wall on the smaller major radius side of the torus. This is one of the main reason for adopting high current density (40 A/mm^2) superconducting coils, which leads to smaller helical coils and hence a larger clearance between the plasma and the wall. Further minor adjustments of B, R, and α will be made to have a clearance of > 3cm.

We describe a few other features of the divertor magnetic configuration. An axisymmetric field changes the size and position of the outermost closed flux surface, but it alters very little the position of the diverting field lines near the divertor plate, i.e. helical coil current essentially determines the position of the divertor channel regardless of the plasma shape, position and the diverting field lines intersect the nearly same position at the divertor plate for two configurations with different axis positions (Δ=0, Δ=-15cm). With increasing α, the closed outermost flux surface becomes larger but the ergodic region becomes narrower, leading to a larger clearance between the divertor plasma and the wall (Fig. 7 (c), (d)). However there is a limit on α above which theoretically achievable $\bar{\beta}$ value suddenly drops. In this sense, α=0.1 is acceptable, but α=0.2 is not.

Another important feature is that the connection length between the main plasma scrape-off layer and the divertor plate is very short (~1m) compared with that of a comparable size tokamak (~10m).

Tokamak divertor experiments have shown that the effective divertor functions require a divertor configuration with high

plugging efficiency, i.e. plasma in the divertor channel "plugs" neutrals recycled at the divertor plasma through ionization process, thus minimizing the neutral flux into the main plasma. This is particularly important for creation of the high density, cold divertor plasma and for access to the H-mode regime [7]. The plugging efficiency depends on the divertor geometry and the divertor plasma (particularly density). Compared with a tokamak divertor, the divertor density for the helical divertor channel is lower for a given average main plasma density [8]. For a helical divertor configuration, its shorter connection length causes faster parallel particle transport in the divertor channel, lowering the divertor density. Lower density makes the plasma plugging more difficult and therefore a more elaborate design of the baffle plate is needed.

Fig.8 shows examples of conceptual baffle plate designs. The design in Fig.8(a) is the simplest, but it interferes with the neutral beam injection and the various diagnostics systems. The design in Fig.8 (b) enhances the plugging efficiency, while avoiding the interference problems. In Fig.8(c), the additional baffle plate are added at the main plasma boundary to increase ionization probability of the neutrals (which escapes from the divertor chamber) outside the outermost closed surface near the X-point. We are also considering a divertor operation mode in which the pump system installed in the divertor chamber pumps the recycled neutrals.

With such baffle plates, we expect that high plugging efficiency can be achieved when the average density is above $5\times10^{13}cm^{-3}$. If so, the following divertor function will help to improve plasma performance in the LHD.

(1) A high density cold divertor plasma is formed just in front of the divertor plate, lowering impurity sputtering from the plate [9]. Even if the impurities are sputtered, they are likely to be ionized in the divertor channel and be swept toward the plate by the plasma flow [10].

(2) High density, cold divertor plasma enhances the radiation power, thus lowering the heat flux on the divertor plasma. This is a divertor function which is necessary for a long pulse or steady state operation of the discharge.

(3) Enhanced recycling at the divertor region makes pumping of the particle and hence the plasma density control easier.
(4) Particle recycling can be localized within the divertor region. This is an important condition for creation of an H-mode tokamak discharge and thus an improved confinement regime may also be obtained even in a helical discharge.

5. HEATING SYSTEM

An ECH system is prepared for initial plasma production and heating. NBI and ICRF heating methods will be used for additional heating [11]. Specifications for the heating systems are summarized in Table 2. The requirements are those needed to achieve the target plasma parameters. An example of experimental layout of the heating systems is shown in Fig.17 in section 6.

The heating systems which require R&D programs are: (i) High-power gyrotron and wave guide system, (ii) Negative ion source in NBI, and (iii) Launcher system in ICRF heating. These R&D programs should be consistent with the experimental schedule. All devices must be designed for use in the high-power, long-pulse operation.

Extensive numerical studies have been carried out to optimize the heating system design. Through these analyses, the following problems have become clear.

(i) According to Monte Carlo calculations of NBI heating, the thermalization rate of perpendicularly injected particles (H^0: 100keV) is very small for the m=10 configuration. On the other hand, tangentially injected particles are well thermalized. Above 60% of the port-through power is expected to be thermalized inside the half-radius of the plasma column. Fig.9 (b) shows the fraction of the port-through neutral beam power thermalized within r/a=1/2 as a function of injection angle.
(ii) With tangential injection, a beam energy of H^0:100keV (D^0:200keV) is necessary to concentrate the absorbed power within the half-radius effectively. At this injection energy, about 60% of the port-through power is deposited within the half-radius of the plasma column at both high and low electron densities (Fig.9(c), (d)).
(iii) For the ICRF (fast-wave) heating, the m=10 magnetic field

configuration has some difficulties for efficient heating due to the large loss-cone in velocity space. Fig.(10) shows an example of the power distribution for the m=10 configuration with loss cone even at the center (T_e=T_i=2keV, $\bar{n}$=$10^{20}m^{-3}$, hydrogen mixing ratio=5%). More than 50% of the input ICRF power is lost through the orbit loss. This orbit loss is reduced down to 30% for the ^3H_e minority case.

Confinement of the high energy particle depends on the magnetic configuration. The radius of the core plasma without loss cone (r_{LC}) increases when the plasma is moved inwards as discussed in Section 3. Fig.10 (b) shows dependence of the power loss on r_{LC}. When there is no loss cone within a third of the plasma radius, the power loss due to orbit loss is below 30% of the input power.

6. EXPERIMENTAL PLAN

The main experimental objective of this project is to investigate the fundamental properties of helical plasmas in the wide range of plasma parameters shown in Fig.11 using advanced heating and diagnostic systems. The other feature of the plan is to make full use of a flexible magnetic field configuration to study effects of various magnetic field characteristics such as ι, magnetic well (or hill) and shear. The flexible magnetic field can be obtained by changing the current profile in the helical coils, the vertical field, and the multipole field. Examples of varying the current profile in the helical coils and the vertical field are shown in Figs.12 and 13, respectively.

A flow chart of planning experiments is shown in Fig.14. Detailed experimental plans for the main subjects of investigation are as follows:

(1) High n τ T regime:

This is the standard operation regime in the helical system, where the density is so high that $T_e \sim T_i$ is valid. ($\bar{n}_e$=$10^{20}m^{-3}$, $\overline{T} \sim$ 3keV)

By investigating confinement characteristics in this regime, and by comparing the results from other smaller devices such as Wendelstein 7A, Heliotron E, CHS, ATF, and Wendelstein 7AS,

confinement scaling including size and B dependence will be experimentally established.

Initial Plasma B=4T, $\bar{n}_e=10^{20}m^{-3}$, $\bar{T}$=0.5-1keV
ECH 112GHz, 3MW
RF 0.5GHz, 5MW
Additional Heating
$\bar{n}_e=10^{20}m^{-3}$, $\bar{T}$=3-4keV
NBI H:125kV, 15MW
(D:250kV, 15MW)
ICRF 60MHz 10MW

(2) High T_i regime

This is a new parameter regime for the helical system, where a low-density, high-temperature plasma is expected. ($\bar{n}_e=10^{19}m^{-3}$, $T_i(0) \sim 10$ keV)

The notable feature of this regime is that the electric field in the plasma becomes positive due to the dominant electron transport. The confinement properties in the low collisionality region can be studied.

Initial Plasma B=4T, $\bar{n}_e=10^{19}m^{-3}$, $\bar{T}$=3keV
ECH 112GHz, 3MW
Additional Heating
$\bar{n}_e= 1 \sim 2\times10^{19}m^{-3}$, $T_i(0) \sim 10$ keV
NBI H:125kV, 15MW
(D:250kV, 15MW)
ICRF 60MHz 10MW

(3) Attainment of high-beta plasma

Although this is one of the fundamental subject in toroidal plasmas, comprehensive experimental studies in this area have not yet been carried out in helical systems. Therefore, this subject should be clarified in the experiment of the next large helical device. The experiment will be done at low magnetic field. In this case, it should be examined whether ECH in low field can produce a high-density plasma, and whether high-energy beam-injected ions can be well confined.

Initial Plasma B = 0.5 ~ 1.0T, $\bar{n}_e=10^{19}m^{-3}$, $\bar{T}$=1keV

ECH 28GHz, 1MW

Additional Heating

$\bar{n}_e= 10^{20}m^{-3}$, $\bar{T}$=1keV

NBI H:125kV, 15MW

(D:250kV, 15MW)

(4) Confinement of long-pulse (steady-state), high temperature plasma

The purpose of this study is to demonstrate confinement of high-temperature plasma for long pulses (or steady state) on time scales much longer than the characteristic time shown in Table 3. The relationship between the diffusion time of a magnetic field and the operation time of a device is shown in Fig.15(a). The n-T diagram for long-pulse operation is shown in Fig.15(b). Making the best use of the device, the following subjects will be studied.

Initial Plasma $\bar{n}_e= 0.5 \sim 10^{19}m^{-3}$, $\bar{T}$=1 ~ 2keV

ECH 112GHz, 3MW, CW

NBI or ICRF 5MW, 100s

If steady-state or quasi-steady-state operation is possible, then helical magnetic field, vertical field, and quadruple field can be fine-tuned on a slow time scale. Transition from the ion root to the electron root can be also studied.

The scenario for steady-state operation will be established through the following items as shown in Fig.16.

(a) Gas fueling, Pellet injection
(Density profile control),

(b) Heating, Slowing down of high-energy particles such as NBI fast ions (Heating power control),

(c) High-temperature, high-density plasma
(Control of Equilibrium)

(d) Plasma ---Recycling with chamber wall, Impurity transport and accumulation,

(e) Divertor --- Particle flux control, Heat flux removal.

These items are coupled in a complicated manner so that long pulse operation is necessary for establishing appropriate external control of each item. Engineering aspects of the control in a

steady-state fusion reactor are expected to be clarified in the LHD with the divertor system.

(5) Confinement of high-energy particles and α -particle simulation.

The objectives are to study confinement of high-energy particles, the transfer of energy from high-energy particles to bulk plasma, and confinement properties of high-energy particles in a nonaxisymmetric system such as heliotron/torsatron type system.

The following subjects, which are closely related to heating method, will be studied:

(a) High-energy NBI with variable injection angle and its absorption efficiency.

(b) Simulation experiments of α - particles in a D-T reactor plasma by producing high-energy He^3 ions with high-power ICRF heating in a D-He^3 plasma.

Table 4 shows a tentative experimental schedule and Fig.17 shows an example of the set-up of the experiment.

Acknowledgements

This design study has been done with the help of researchers and engineers in Japanese universities and industry. We would like to express our particular appreciation to the theory group of Oak Ridge National Laboratory (US), who has generoulsy provided us various codes, which have been used in optimizing the magnetic configuration.

References

1. B.A. Carreras, G. Grieger, J.H. Harris, J.L. Johnson, J.F. Lyon et al. "Progress in Stellarator/Heliotron Research" Nucl. Fusion 28 (1988) 1613.
2. J. Todoroki, T. Kamimura, H. Sanuki, T. Amano, T. Hayashi et al., "MHD and Transport study of ℓ=2 Heliotron/Torsation." 12th International Conference on Plasma Physics and Controlled Nuclear Fusion Research (Nice, 1988) IAEA-CN-50/C-5-4.
3. S. Sudo, Y. Makeiri, H. Zushi, F. Sano, K. Itoh et al. "Scalings of Energy Confinement and Density Limit in Stellarator/Heliotron" PPLK-R-40 (1989).
4. Y. Nakamura and M. Wakatani. "Transport Simulations of New Stellarator/Heliotron" PPLK-R-24 (1988)
5. O. Motojima, K. Yamazaki, T. Mutoh, Y. Takeiri, T. Kuroda et al., "Engineering Desigh Study of the Large Superconducting Helical Device." Fusion Technology 1988, Vol.1 p.402-406.
6. K. Yamazaki, O. Motojima, S. Morimoto, K. Nishimura, T. Mizuuchi et al., "Comparative Design Study of Super -vs. Normal Conducting Large Helical Device." Fusion Technology 1988, Vol.1 p.407-411.
7. F. Wagner, G. Becker, K. Behringer, D. Campbell, A. Eberhagen, et al., "Regime of Improved Confinement and High Beta in Neutral-Beam-Heated Divertor Discharges of the ASDEX Tokamak." Phys. Rev. Lett. 49 (1982) 1408.
8. T. Obiki, T, Mizuuchi, H. Zushi, K. Kondo, F. Sano et al., "Recent Experiments on Heliotron E." 12th International Conference on Plsma Physic and Controlled Nuclear Fusion Research (Nice 1988), IAEA-CN-50/C-1-1.
9. M.A. Mahdavi, J.C. DeBoo, C.L. Hsieh, N. Ohyabu, R.D. Stambaugh, J.C. Wesley, "Particle Exhaust from Plasma Discharges weith an Expanded Boundary Divertor." Phys. Rev. Lett. 47 (1981) 1602
10. N. Ohyabu, J.C. DeBoo, R.J. Groebner, C.L. Hsieh, M.A. Mahdavi et al., "Effect of Divertor Geometry on Impurity Exhaust", Nucl. Fusion 23 (1983) 295.
11. T. Mutoh, Y. Takeiri, T. Obiki, F. Sano, A. Fukuyama et al., "Heating System of Large Superconducting Helical Device." Fusion Technology 1988, Vol.1 p.552-556.

Figure Captions

Fig.1 a) Overview of Large Helical Device
b) Cross section of LHD at three different toroidal angle.
From the left, 0°, 18°, 9°
c) Experimental facilities of LHD.

Fig.2 Contours of constant β_{eq} (MHD equilibrium beta limit), β_{st} (MHD stability beta limit), ι_s (ι at the outer most closed surface), ε_h (helical ripple), A_p (plasma aspect ratio) and A_c (helical coil aspect ratio) are shown in the coil parameter (γ_c, m) space. The crossed hatched areas are the practical range of γ_c when m=10 or m=14.

Fig. 3 Equilibrium beta limit $\overline{\beta}_{eq}$ (dotted line) and stability beta limit $\overline{\beta}_{st}$ (solid line) versus plasma position.
(a) for m=10/ γ_c=1.20 / R=4m case. (b) for m=14 / γ_c=1.25 / R=5m case.

Fig. 4 Dependence of ε_h and S_p/S_c on γ_c.

Fig. 5 Parameter space of the target plasma.
The cross hatched area are the expected parameter space for a case (a_p=0.6m, R=5m, B=4T, P_{abs}=19MW).
Various Curves at the cross hatched area are the predictions from τ_E^{EMP1} scaling, τ_E^{EMP2} scaling, neoclassical transport plus anomalous transport ($\chi_{ano}=6\times10^{18}/n$ m^2/s) and neoclassical transport alone.

Fig. 6 Particle loss diagram in pitch angle and major radius, at the toroidal angle 18° for m=10 configuration. The position of the magnetic axis is shown by dagger, and the outermost magnetic surface by triangles. Passing (P), locally-trapped(LT), and quasi-trapped (QT)

particles are classified in this figure. (b) Particle loss fraction versus position of magnetic axis. The square shows $m=10/\gamma_c=1.20$ / R=4m case and the circles shows $m=14/\gamma_c=1.25$ / R=5m case.

Fig. 7 Variation of divertor magnetic configuration due to coil pitch modulation (α) and shift (Δ) ($\ell=2$, $m=10$, $\gamma_c=1.2$)

Fig. 8 Examples of the baffle plate designs

Fig. 9 a), b) Power absorption efficiency and thermalization efficiency of the neutral beam heating (H^0, 100keV) for high n τ T operation regime
($B=4T$, $\bar{n}=10^{14}(1-(r/a)^2)^{0.5}cm^{-3}$)
a) fraction of the port-through neutral beam power absorbed within r/a=1/2.
b) fraction of the port-through neutral beam power thermalized within r/a=1/2.
c),d) Dependence of NBI power absorption efficiency on beam energy (tangential injection, 53°),
o: power absorption efficiency,
Δ: shine through power
c) $n(r)=3x10^{13}(1-(r/a)^2)cm^{-3}$
d) $n(r)=1x10^{14}(1-(r/a)^2)^{0.5}cm^{-3}$ (by K. Hanatani)

Fig. 10 a) Loss power and heating power distribution for the configuration with loss cone at the center
b) Dependence of the power loss on the radius of the core plasma with out loss cone (r_{LC}) (by A. Fukuyama)

Fig. 11 Target plasma parameter region
ν^{**} is defined as $\nu R/(\varepsilon_h^{3/2} m v_{th})$

Fig. 12 Change of the magnetic surface due to variation of the current distribution in the helical coil. The helical coil current flows at the solid dots.

Fig. 13 Variation of the magnetic field characteristics due to change in the vertical field for a case (ℓ=2, m=12, R_0=4.8m, a_c=0.96m, γ_c=1.2, B=4T and coil width 80cm/thickness 45cm/width modulation rate 0.5). R_{in} and R_{out} are the radial positions (relative to R_0=4.8m) of the outermost closed surface at ϕ= 0° on the smaller major radius and larger major radius sides respectively.

Fig. 14 Flow chart of planning experiments.

Fig. 15 a) relation between diffusion time of magnetic field and operation time.
b) n-T diagram in the long-pulse operation mode.

Fig. 16 Scenario of steady-state operation.

Fig. 17 Example of experimental set-up.

Table 1 Construction Schedule of the LHD.
Table 2 Heating methods and specification.
Table 3 Characteristic time and physics subjects.
Table 4 Schedule of experiments.

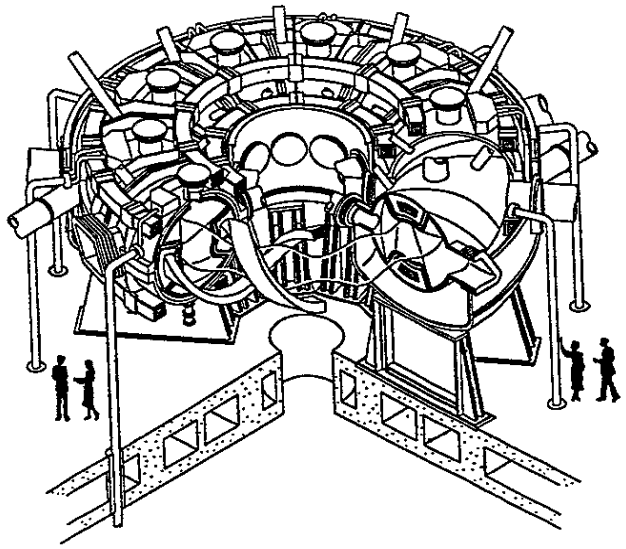

Fig.1 a) Overview of Large Helical Device

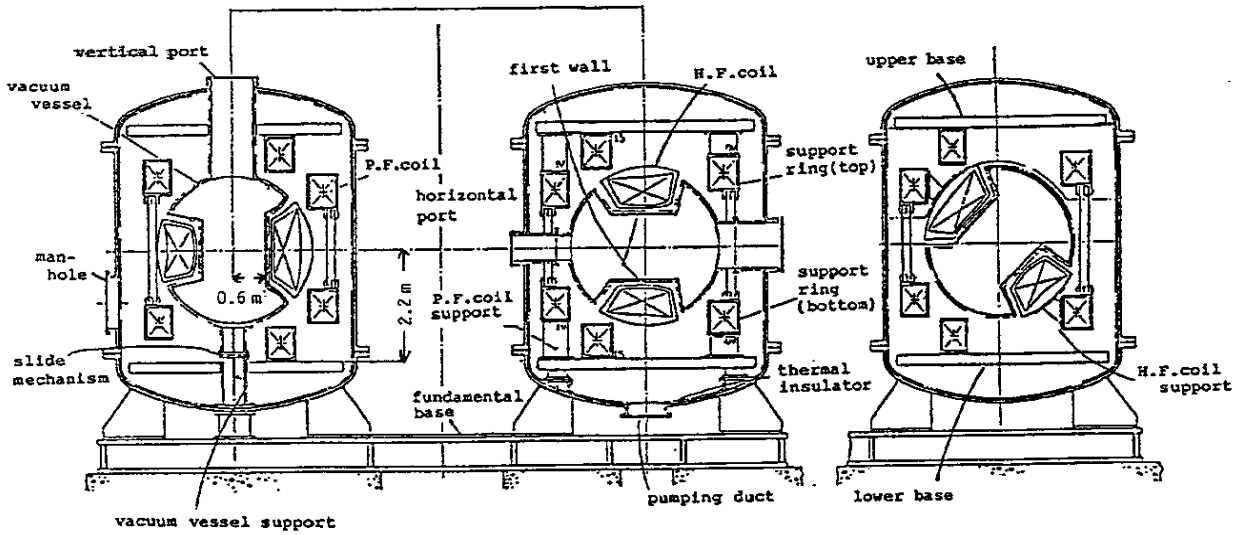

Fig.1 b) Cross section of LHD at three different toroidal angle.
From the left, 0°, 18°, 9°

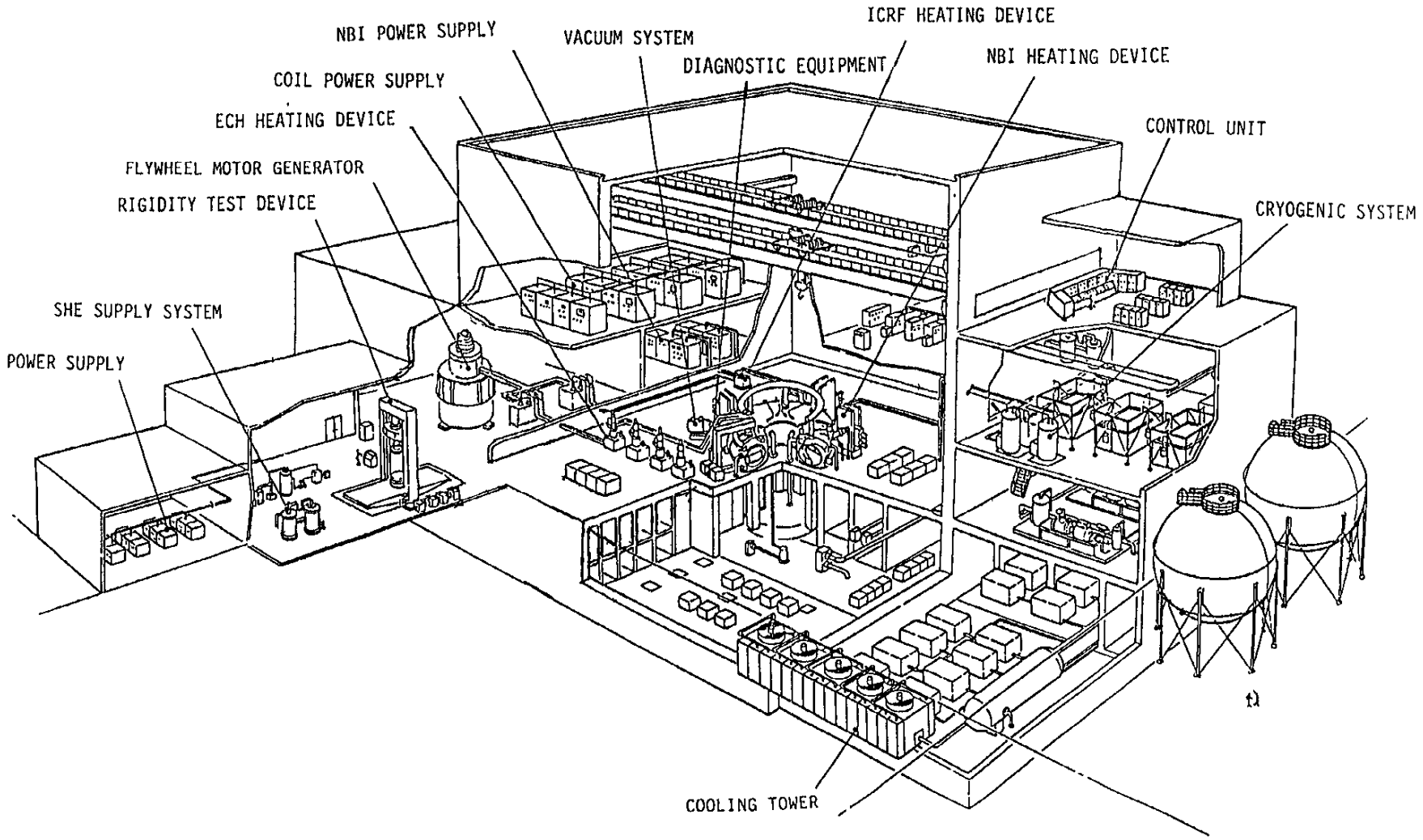

Fig.1 c) Experimental facilities of LHD.

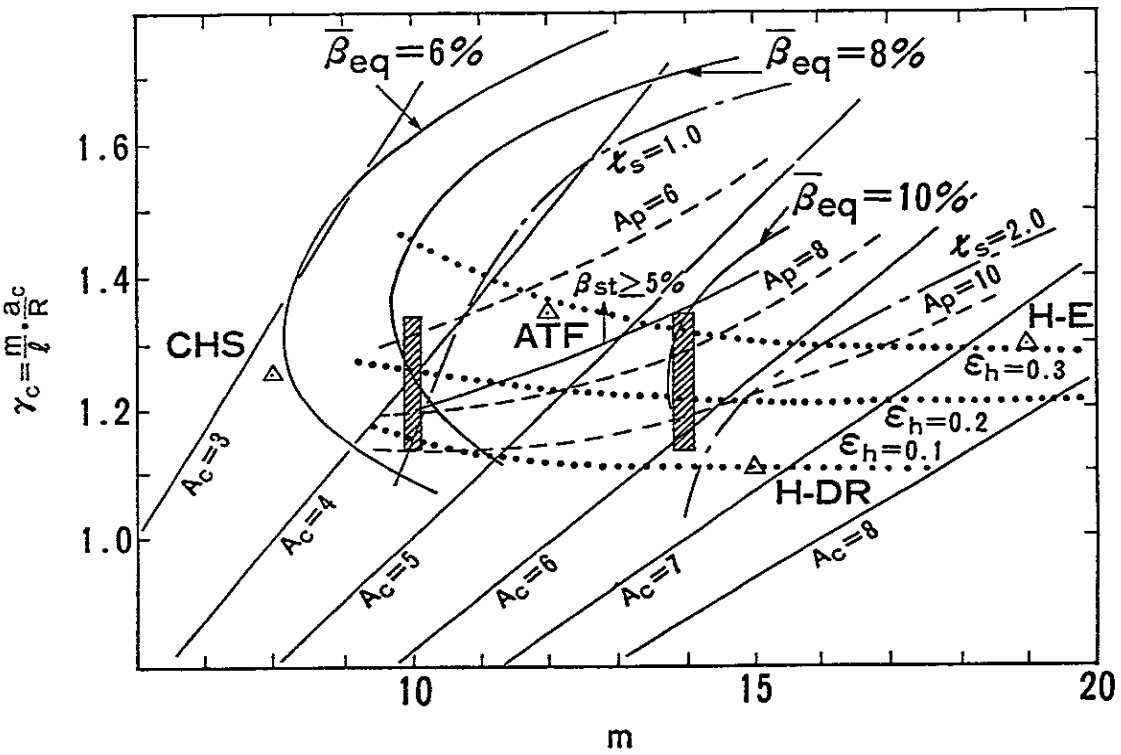

Fig.2 Contours of constant β_{eq} (MHD equilibrium beta limit), β_{st} (MHD stability beta limit), ι_s (ι at the outer most closed surface), ε_h (helical ripple), A_p (plasma aspect ratio) and A_c (helical coil aspect ratio) are shown in the coil parameter (γ_c, m) space. The crossed hatched areas are the practical range of γ_c when m=10 or m=14.

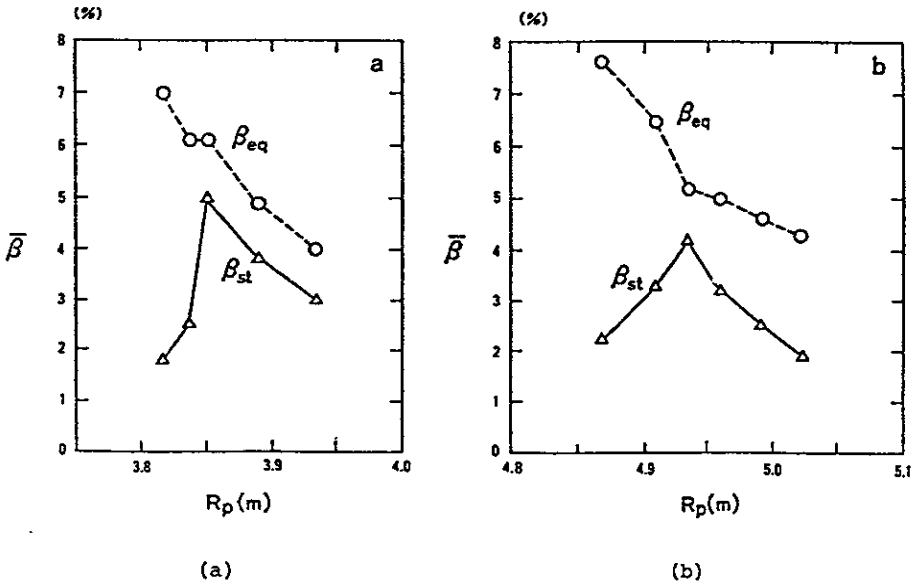

Fig.3 Equilibrium beta limit $\bar{\beta}_{eq}$ (dotted line) and stability beta limit $\bar{\beta}_{st}$ (solid line) versus plasma position.
(a) for m=10/ γ_c=1.20 / R=4m case. (b) for m=14 / γ_c=1.25 / R=5m case.

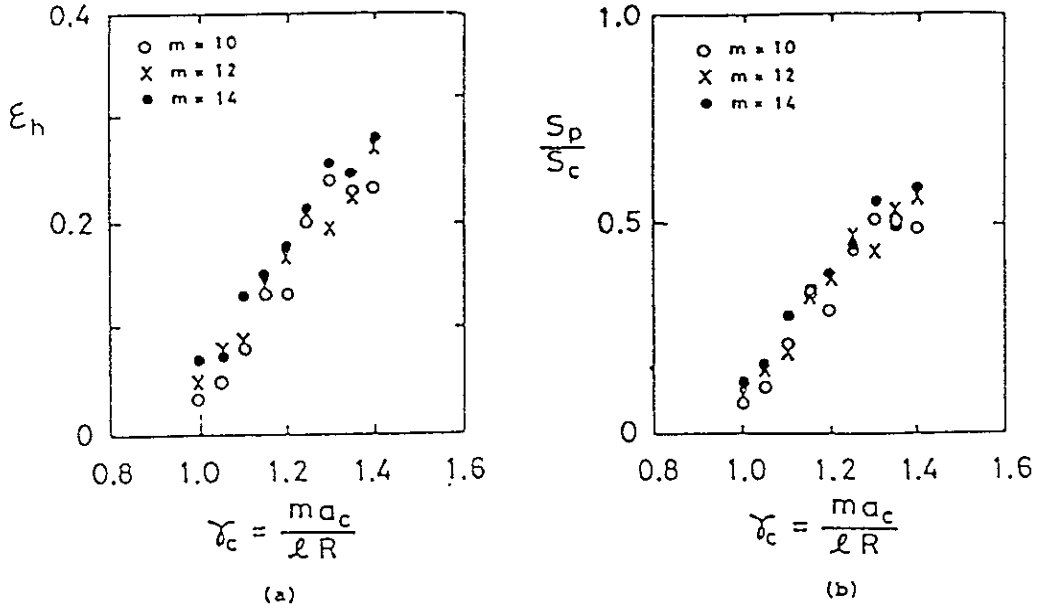

Fig.4 Dependence of ε_h and S_p/S_c on γ_c.

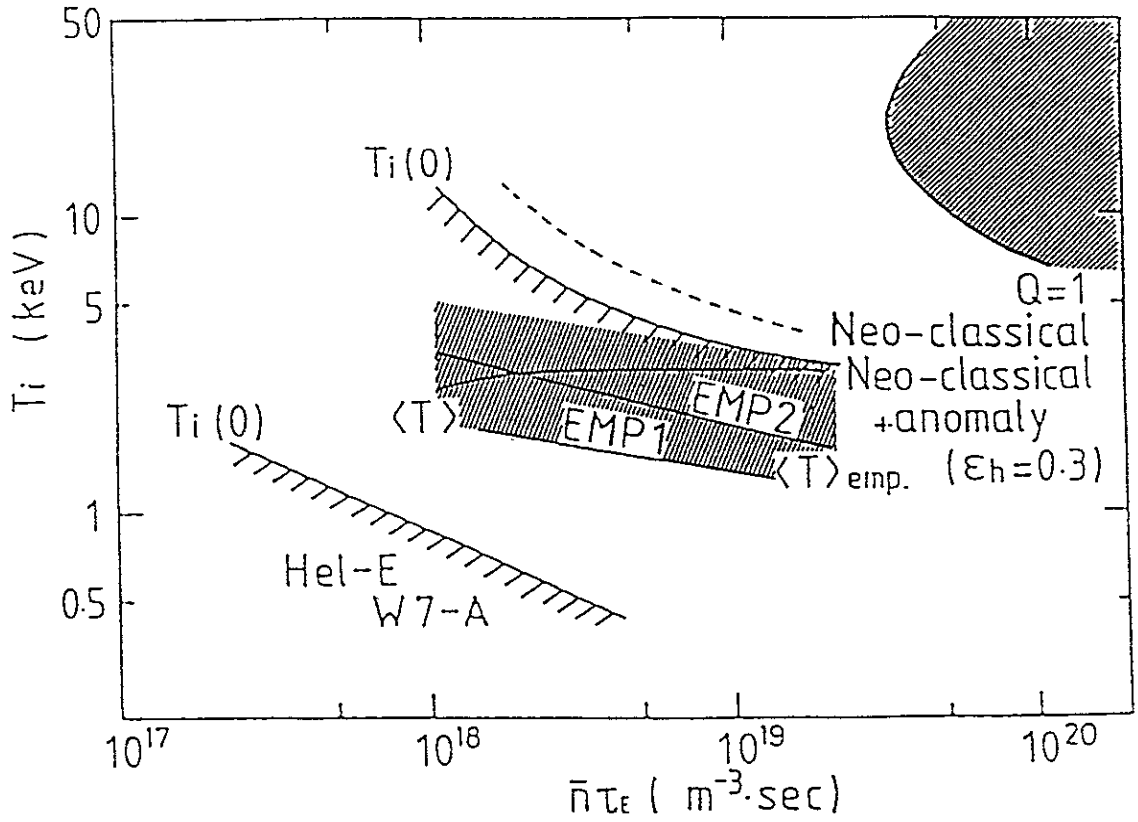

Fig.5 Parameter space of the target plasma.
The cross hatched area are the expected parameter space for a case (a_p=0.6m, R=5m, B=4T, P_{abs}=19MW).
Various Curves at the cross hatched area are the predictions from τ_E^{MP1} scaling, τ_E^{MP2} scaling, neoclassical transport plus anomalous transport ($\chi_{ano}=6\times10^{18}/n$ m^2/s) and neoclassical transport alone.

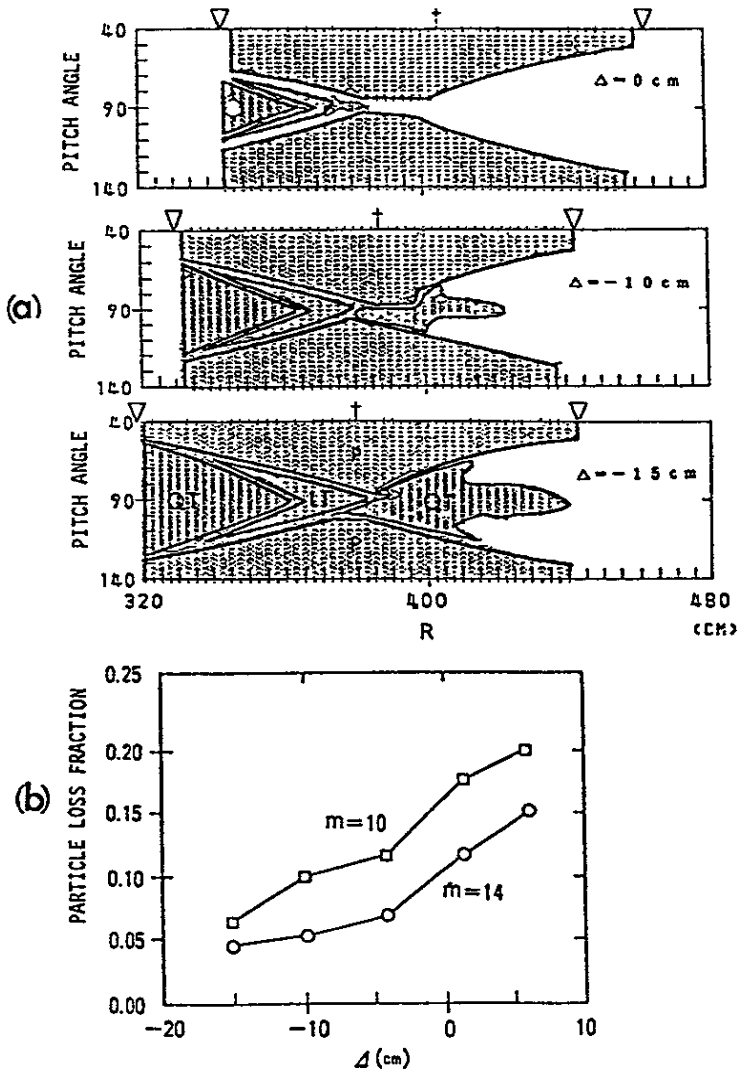

Fig.6 Particle loss diagram in pitch angle and major radius, at the toroidal angle 18° for m=10 configuration. The position of the magnetic axis is shown by dagger, and the outermost magnetic surface by triangles. Passing (P), locally-trapped(LT), and quasi-trapped (QT) particles are classified in this figure. (b) Particle loss fraction versus position of magnetic axis. The square shows $m=10/\gamma_c=1.20$ / R=4m case and the circles shows $m=14/\gamma_c=1.25$ / R=5m case.

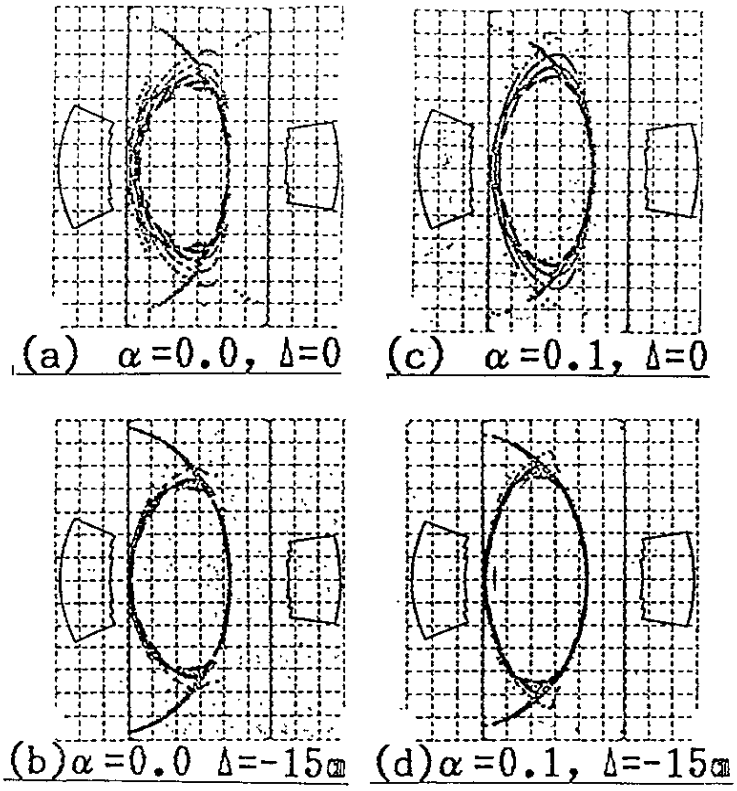

Fig.7 Variation of divertor magnetic configuration due to coil pitch modulation (α) and shift (Δ) (ℓ=2, m=10, γ_c=1.2)

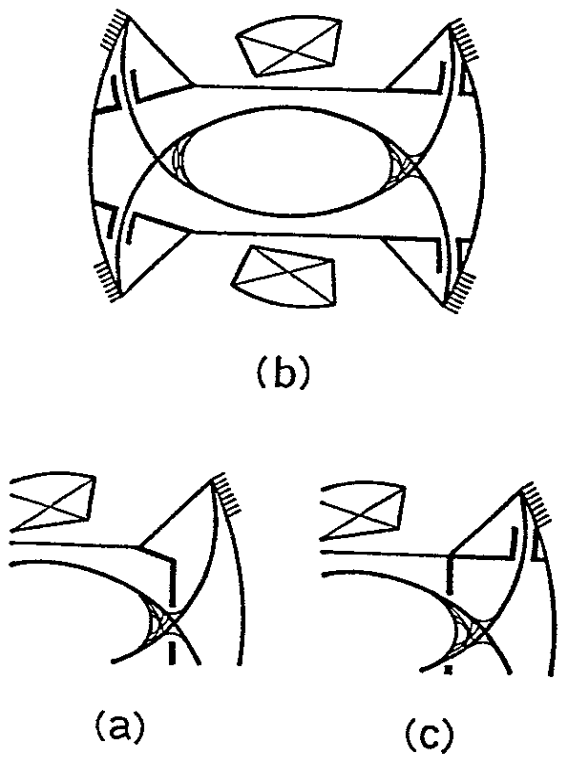

Fig.8 Examples of the baffle plate designs

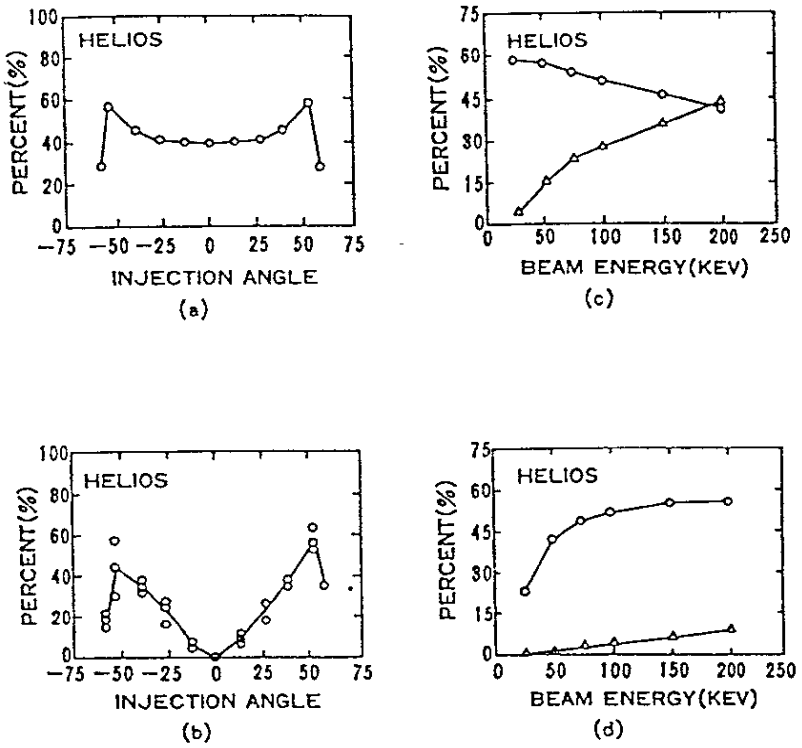

Fig.9 a), b) Power absorption efficiency and thermalization efficiency of the neutral beam heating (H^0, 100keV) for high n τ T operation regime
($B=4T$, $\bar{n}=10^{14}(1-(r/a)^2)^{0.5}cm^{-3}$)
a) fraction of the port-through neutral beam power absorbed within $r/a=1/2$.
b) fraction of the port-through neutral beam power thermalized within $r/a=1/2$.
c),d) Dependence of NBI power absorption efficiency on beam energy (tangential injection, 53°),
o: power absorption efficiency, Δ: shine through power
c) $n(r)=3x10^{13}(1-(r/a)^2)cm^{-3}$, d) $n(r)=1x10^{14}(1-(r/a)^2)^{0.5}cm^{-3}$
(by K.Hanatani)

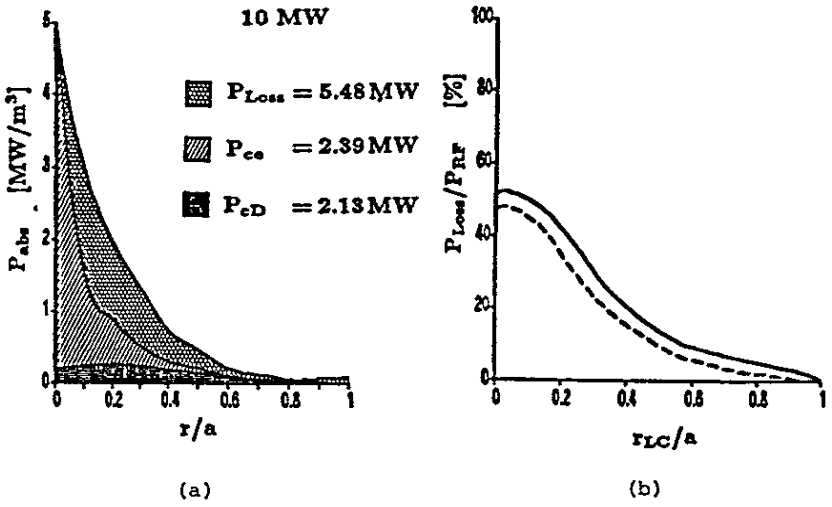

Fig.10 a) Loss power and heating power distribution for the configuration with loss cone at the center
b) Dependence of the power loss on the radius of the core plasma with out loss cone (r_{LC}) (by A. Fukuyama)

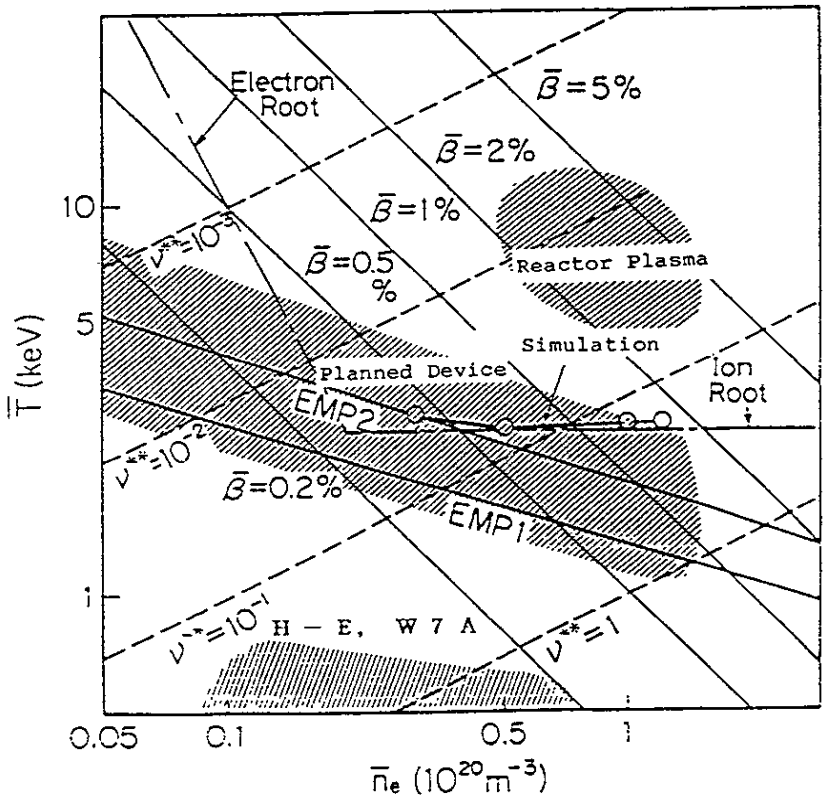

Fig.11 Target plasma parameter region
ν^{**} is defined as $\nu R/(\varepsilon_h^{3/2} m v_{th})$

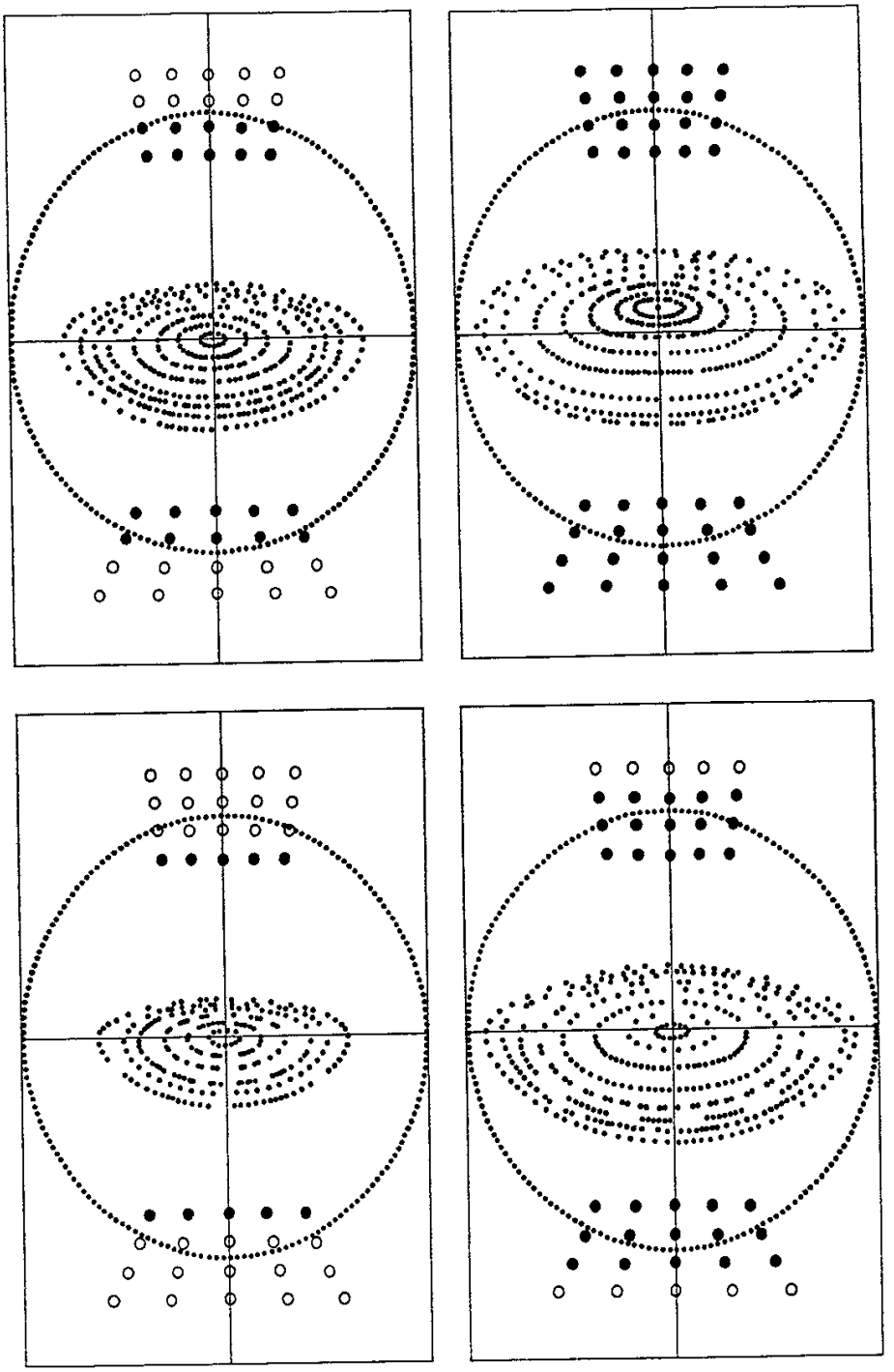

Fig.12 Change of the magnetic surface due to variation of the current distribution in the helical coil. The helical coil current flows at the solid dots.

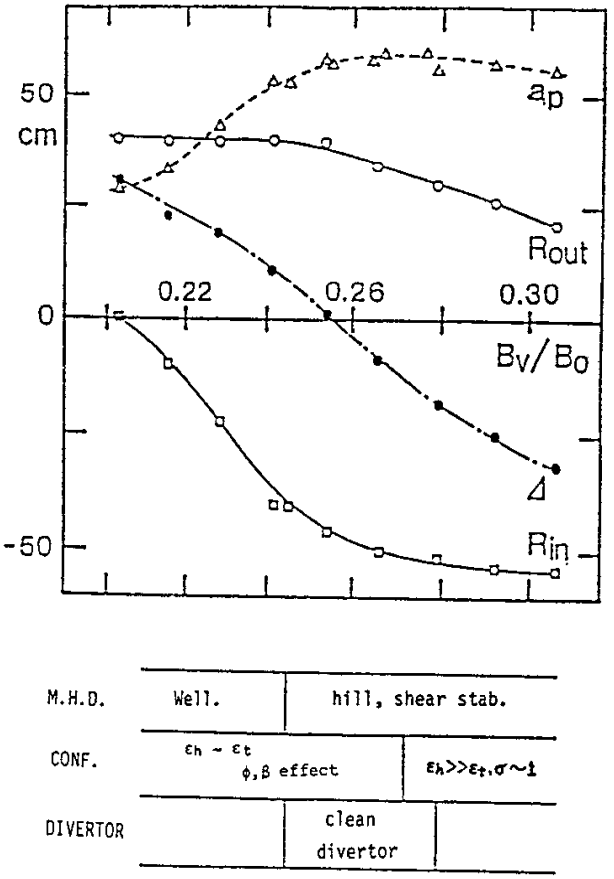

Fig.13 Variation of the magnetic field characteristics due to change in the vertical field for a case (ℓ=2, m=12, R_0=4.8m, a_c=0.96m, γ_c=1.2, B=4T and coil width 80cm/thickness 45cm/width modulation rate 0.5). Rin and Rout are the radial positions (relative to R_0=4.8m) of the outermost closed surface at φ=0° on the smaller major radius and larger major radius sides respectively.

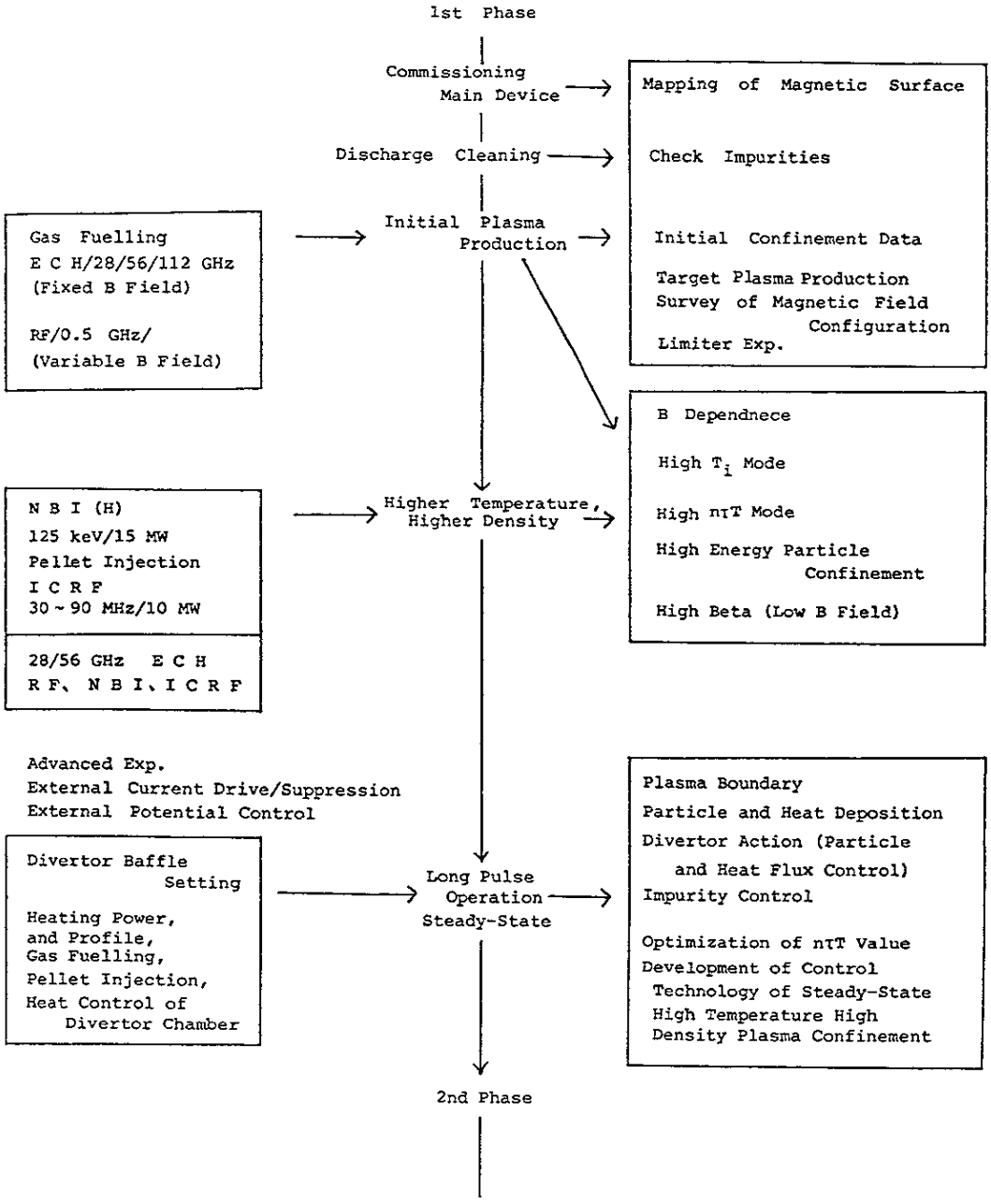

Fig.14 Flow chart of planning experiments.

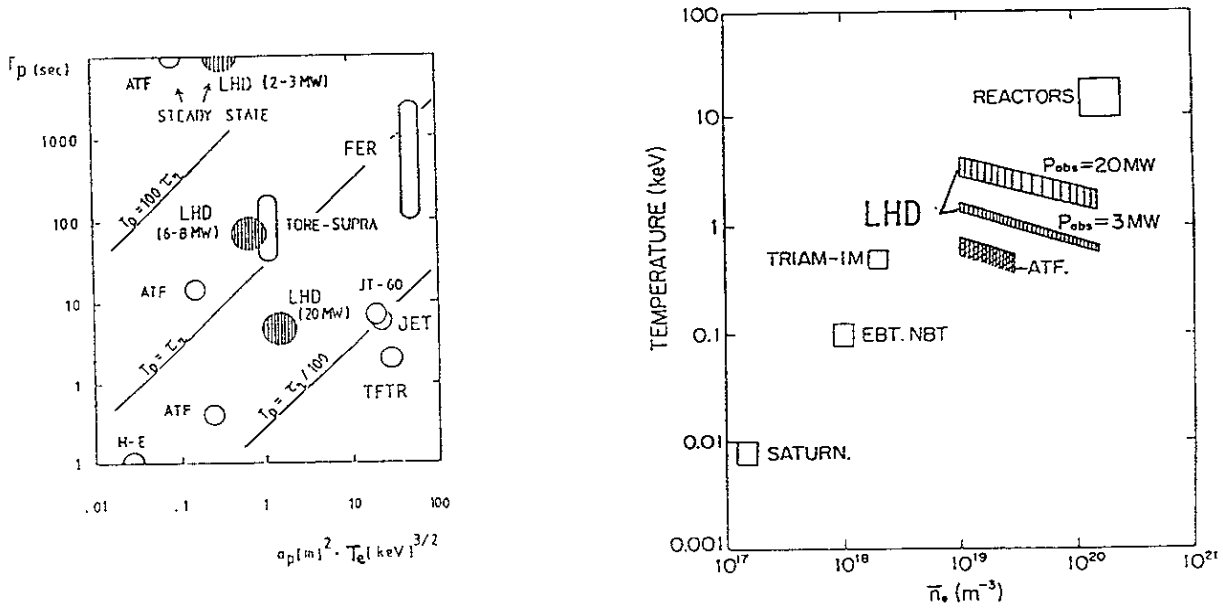

(a) (b)

Fig.15 a) relation between diffusion time of magnetic field and operation time.
b) n-T diagram in the long-pulse operation mode.

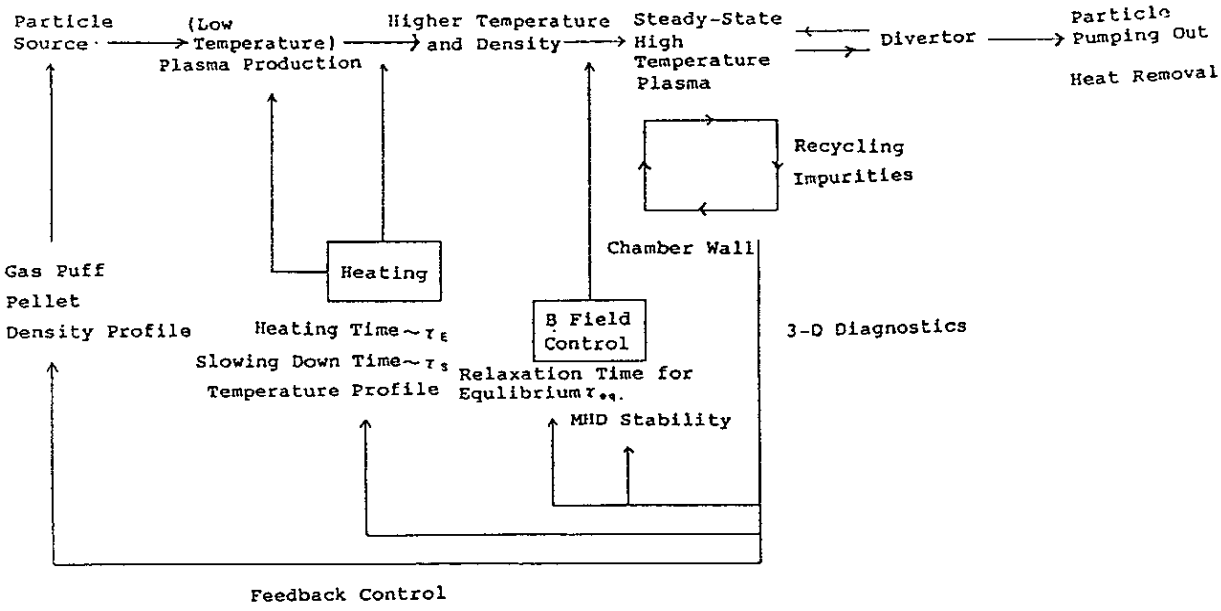

Fig.16 Scenario of steady-state operation.

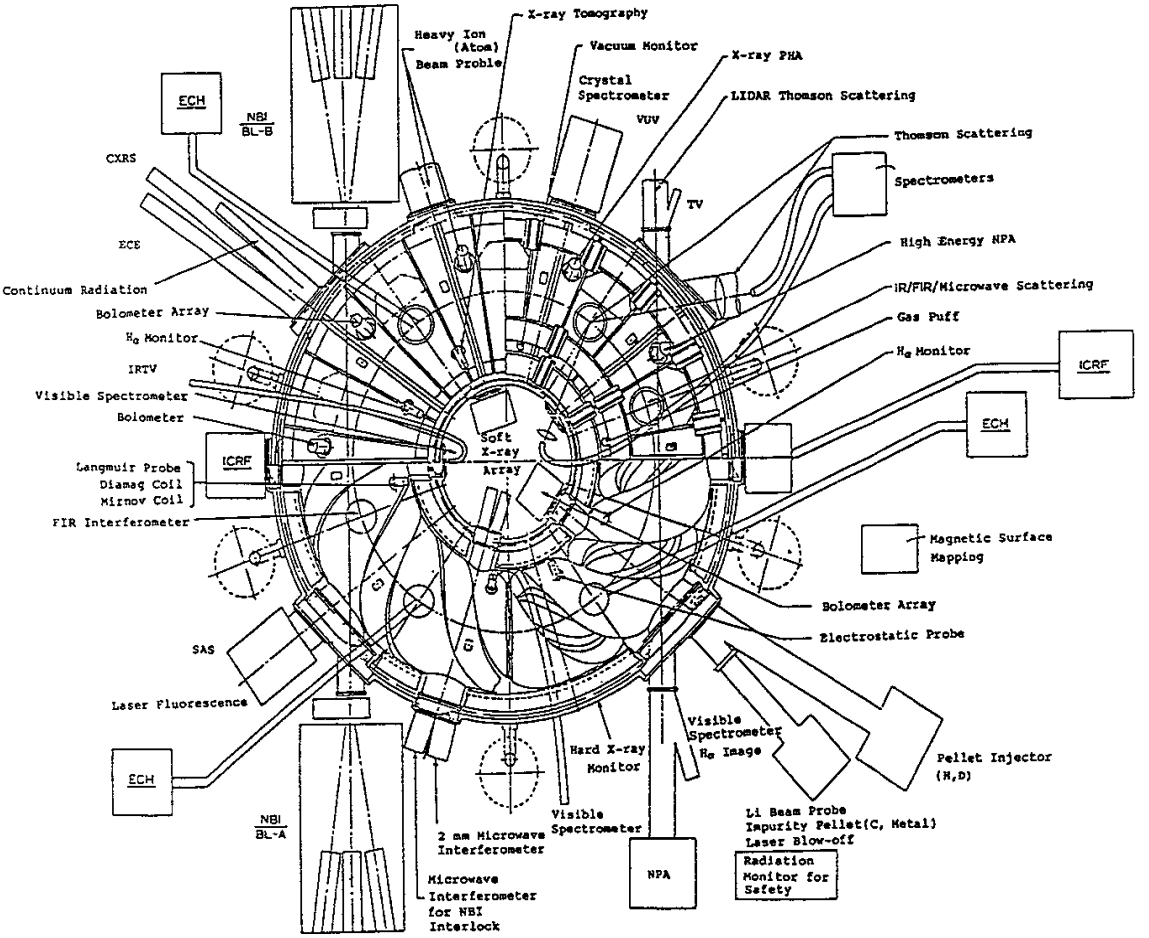

Fig.17 Example of experimental set-up.

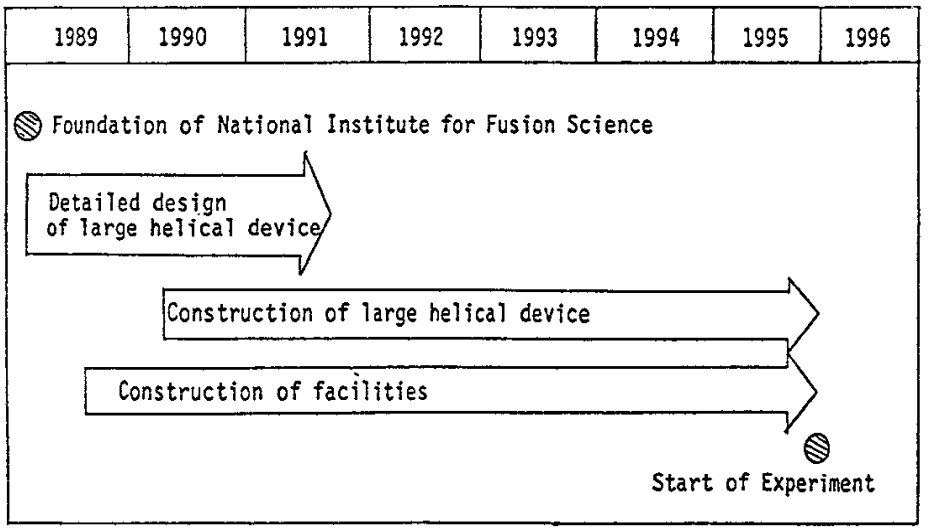

Table 1 Construction Schedule of the LHD.

Heating Method and Specification

	Objectives	Specification	Feature and Necessity
Category 1 ECH	• Target Plasma Production • Transport • (Electron Root)	• Frequency ~100GHz ~56GHz • Output Power 5~10MW 400kW • Pulse Width 10sec~CW CW	• Established Method for Plasma Production and Heating • Development of Waveguide is Necessary
NBI	• Heating at High Density Region • Achievement of Target Parameters • Production of High-$n\tau T$, High-T_i and High-β Plasma	• E_0= 75~125 keV(H°), (150~250 keV(D°)) • P_{NBI} ~20 MW Port-through • Beam Line Numbers 2(D° beam) 4(H° beam) • Ion Source Positive or Negative • Pulse Width ~10 sec(20 MW) ~30 min(4~5MW)	• Established Method for Additional Heating.
Category 2 ICRF	• Fast-wave Heating • IBW Heating • High-T_i Modes • Simulation of Nuclear Reaction	• Frequency 30~90 MHz(Variable) • Output Power 15 MW • Pulse Width ~10 sec(15MW) ~CW (5 MW)	• Established Method in Large Tokamaks • Construction Cost Per Power is Cheaper than NBI • Development of Antenna is Necessary
LHCD	• Current Drive/Suppression	• Frequency ~3.7 GHz • Output Power ~5 MW • Pulse Width ~100 sec	• Relation between Current and Confinement • Development of Launcher is Necessary
Whistler Wave	• Plasma Production Independent of B Field	• Frequency ~500 MHz • Output Power ~5 MW • Pulse Width ~10 sec	• Experiments independent of B Field Strength • Optimization of Antenna.

Category 1: For Achievement of Plasma Parameters Category 2: For study of Physics

Table 2 Heating methods and specification.

Characteristic Time and Physics Subjects

	⟨Characteristic Time⟩		⟨Subjects⟩
10^{-2}s			
	τ_{ei}	(collision)	
	$\tau_{ei}^{E}=m_i/m_e \cdot \tau_{ei}$	(energy relaxation)	
10^{-1}s			
	τ_H	(heating)	
	τ_E	(energy confinement)	Confinement Physics
	τ_P	(particle confinement)	
	τ	(electric field generation)	
5×10^{-1}s			
	τ_{hot}	(high-energy particle confinement)	Reactor
	$\tau_{hot\,sl}$	(〃 slowing down)	Simulation
$\lesssim$1s			
	τ_α	(α-particle generation)	
	$\tau_{\alpha sl}$	(α-particle slowing down)	
	$\tau_{\alpha\varphi}$	(electric field generation due to α-particle)	
5s			
	τ_{imp}	(impurity accumulation)	Impurity Transport Physics
	τ_{wall}	(plasma-wall equilibrium)	Divertor Physics
50s			
	τ_η	(resistive skin time)	Equilibrium Relaxation
$\gtrsim$500s			
	τ (?)	(?)	(?)
			demonstration of steady-state operation

Table 3 Characteristic time and physics subjects.

Schedule of Experiments

Period	1	2	3	4	5
Magnetic Field Pulse width	B=4T τ p=2-10sec	B=4T B=1-2T	B=4T Long Pulse	B=4T	B=4T(1-2T)
Experimental Modes	Commissioning Phase Initial Operation (ECH) ECH Exp.	NBI Exp.(High nτT,High Ti) NBI + ICRF Exp.(High nτT) High β Exp.	Divertor Exp. High nτT High β Long Pulse	α-particle Simulation Exp. Current-Related Exp.	Optimized Parameter Exp. Highest Ti Highest nτT Highest β
	Carbon Tile Mapping Discharge Cleaning	Pellet Injection Antenna Setting Divertor Baffle Setting	Impurity Control Long-Pulse Operation	ICRF High-Energy Tail High-Energy Particle Injection D-D Exp. Current Drive/Suppression	Modification of Device Increase Heating Power Data Accumulation for Next Device
Purpose of Experiments	Transport	High β	Divertor	α-particle Simulation	
	Neoclassical Theory:Electron Root, Ion Root ---Exp. Anomalous Transport Effect of Electric Field Confinement of High-Energy Particles	Confinement of High-Energy Particles MHD Theory -- Exp. Currentless Equilibrium Change of Magnetic Field Configuration	Behavior of Impurities Control of Impurities Divertor Action Control of Particle/Heat Flux X-point Configuration	Confinement of High-Energy Particles Simulation of Ash Removal	Highest Parameters High-Power Long-Pulse Exp.
Plasma Parameters	n($10^{20}m^{-3}$) 0.05-0.1 ~1 T(eV) Te(0)~10 T(0)~4 τ (ms) ~100	0.2-0.3 ~1 Ti(0)~10 Ti(0)~2 ~40 <β>~5%	~0.5 ~0.5 ~1 Ti(0)~2 T(0)~5 T(0)~4 ~100		
Heating (Absorbed Power)	ECH 112GHz NBI 125KV(H) 250KV(D) ICRF 60MHz	5MW 10sec 56GHz 15MW 10sec 10MW 10sec	5MW CW (10sec ~) 8MW 5sec, 5MW CW	20MW 10sec, 3MW 30sec 20MW 10sec	

Table 4 Schedule of experiments.